Journal of Fluids and Structures 94 (2020) 102909

Contents lists available at ScienceDirect

Journal of Fluids and Structures

journal homepage: www.elsevier.com/locate/jfs

Linear wave-induced dynamic structural stress analysis of a 2D semi-flexible closed fish cage

Ida M. Strand [a,b,*], Odd M. Faltinsen [a]

[a] Centre for Autonomous Marine Operations and Systems, Department of Marine Technology, Norwegian University of Science and Technology, Trondheim, Norway
[b] Norconsult AS, Trondheim, Norway

ARTICLE INFO

Article history:
Received 29 September 2019
Received in revised form 21 January 2020
Accepted 6 February 2020
Available online xxxx

Keywords:
Hydroelasticity
Beams
Aquaculture
Waves
Sloshing
Stress

ABSTRACT

Closed fish cages in the sea are proposed as a new concept in marine aquaculture, replacing the conventional net cages in order to meet ecological challenges related to fish lice and escapes. A closed fish cage can be compared to a floating tank structure with an internal free surface. Several types of closed cages have been suggested, and they are categorised according to structural properties as flexible membrane structures (fabric), semi-flexible structures (glass fibre) and rigid structures (steel or concrete). To be able to develop safe and reliable structures, more knowledge is required on the seakeeping behaviour of closed cages in waves and the structural response to the wave loads. This paper builds on a theory presented in Strand and Faltinsen (2019) on the linear wave loads on a 2D closed flexible fish cage. A modelling error has been found in Strand and Faltinsen (2019), however, all the main conclusions are in hold. The error has been corrected in the model in the present paper. The present paper extends the model to include bending in the structural model to be able to handle semi-flexible structures where bending stiffness is significant. In this paper, the linear theory of a 2D semi-flexible closed fish cage in waves is developed and analysed to investigate the structural response of the semi-flexible closed cage in waves. We have compared a quasi-static analysis with a fully coupled hydroelastic analysis to investigate if it is a valid and conservative assumption to assume that the stresses in the structure can be assumed quasi-static. If a hydroelastic analysis is necessary or not, is dependent on the stiffness of the structure. We have investigated what happens with the stress in the curved beam part of the closed fish cage for increasing and decreasing stiffness relative to a reference composite structure. One stiffer and two softer cases have been analysed. One major concern for the structural stresses in a closed cage is the effect of sloshing. Sloshing is internal wave motion inside the cage and have multiple resonance periods. The results indicate that to use the quasi-static assumption in structural stress calculation is conservative within the given frequency range for all examined stiffnesses and frequencies, except the frequencies very close to the second sloshing frequency. Close to the second sloshing frequency for all the examined stiffnesses, a localised peak can be observed in the coupled hydroelastic results. The second sloshing frequency is a frequency connected to a symmetric sloshing mode. Rigid body motion is not affected at the symmetric sloshing frequency for an assumed rigid structure, and are therefore also not visible in the stress results from the quasi-static analysis. The structural stress in irregular sea was calculated. These results show no indication of increased stress close to the second sloshing frequency. However, this is not a surprising result since the stress peak is very localised in frequency, and the accumulated effect on the stress standard deviation is therefore small.

* Correspondence to: Klæbuveien 127, 7031 Trondheim, Norway.
E-mail address: ida.marlen.strand@Norconsult.com (I.M. Strand).

https://doi.org/10.1016/j.jfluidstructs.2020.102909

Nomenclature

$A_w(z_e)$	Waterplane area
b_t	Internal distance between the floater at the free surface of the cage
z_B	Coordinate of the centre of the buoyancy
z_G	Coordinate of the centre of gravity
∇	Displaced volume of water of the cage per unit length
ζ^i	Internal wave elevation
IBM	Immersed boundary method

1. Introduction

Norway has become the World's largest producer of Atlantic salmon through the use of open net structures in the sea. The aquaculture facilities have grown in both size and number. Currently, the industry faces increased attention on environmental challenges related to fish escapes, sea lice, diseases, and pollution. A possible solution is to use a floating closed fish cage in the sea. A closed fish cage can be compared to a floating tank structure with an internal free surface. Several types of closed cages have been suggested, and they are categorised according to structural properties as flexible membrane structures, semi-flexible structures and rigid structures based on the degree of deformation of the cage (Kristiansen et al., 2018). Several geometries for the closed cages have been considered by the industry, among them both geometries resembling upright circular cylinders and half spheres.

Limited scientifically published material is available related to the effect of sea loads on closed fish cages. The authors have previously analysed a closed flexible fish cage made of a fabric material. 3D model experiments for both still water (Strand et al., 2014), current (Lader et al., 2015; Strand et al., 2016) and waves (Lader et al., 2017) have been performed, for various filling levels and geometries. Resonant internal water motion (sloshing) was observed in model tests with a closed flexible fish cage both by Solaas et al. (1993) and by Lader et al. (2017). The linear wave response of a 2D closed flexible fish cage was analysed in Strand and Faltinsen (2019). All the results showed that the closed flexible fish cage is flexible, behaves hydro-elastically and that the response is highly dependent on both geometry and filling level. Even less information is available for the rigid and semi-flexible closed fish cages than for the closed flexible fish cage previously investigated by the authors. Kristiansen et al. (2018) ran dedicated model tests of the wave-induced motion of rigid closed cages and compared to numerical simulations using linear potential theory in the frequency domain. The results showed that the influence of sloshing on the rigid body motions was significant. Tan et al. (2019) run non-linear numerical wave response simulations of a rigid cage shaped as an upright circular cylinder. The work was based on linear radiation/diffraction theory for external hydrodynamics and single-dominant multimodal theory (Faltinsen and Timokha, 2009) for sloshing in the cage. They also showed that the sloshing inside the cage was significant and observed both planar wave systems and non-linear swirling inside the cage. No published material has been found related to sealoads on the semi-flexible closed fish cages. However, for rigid and semi-flexible cages, comparisons to ships and offshore structures can be made. Sloshing is an essential phenomenon for closed cages in waves, and here the general theory of sloshing in tanks can be used. Sloshing in tanks have been thoroughly studied in Faltinsen and Timokha (2009) and Ibrahim (2005).

To be able to develop safe and reliable structures, more knowledge is required on the seakeeping behaviour of closed cages in waves and the structural stress response to the wave loads. To the best of the author's knowledge, no previous published works have investigated the structural stresses on any closed fish cage. The emphasis in the present paper will be on the semi-flexible closed cage. Only two-dimensional flow is considered. The semi-flexible closed cage analysed here is assumed made of a glass fibre composite material. It has two floaters on the top, and the bottom beam part is made in a half circular shape, as illustrated in Fig. 1. The material that the closed fish cage is made of is considered impermeable, and any water exchange for the real concept is through pipes. This water exchange is not modelled here.

The dynamics of a real closed fish cage in the sea is three-dimensional. However, to develop theory and understanding of the coupling between structural response, and external and internal wave motions, we start with basics, and the problem is simplified to a 2D problem. A 2D solution will not be representative of existing real-life cage but can be used as a starting point to gather knowledge of the behaviour of this type of structure in waves.

To predict the response of a 2D semi-flexible closed cage in waves three coupled sub-problems must be solved: the structure dynamics, the external problem with incident waves and the effect of the structure on the flow, and the internal problem, which is an internal sloshing problem. It is crucial to understand the dependency between forces and deformations to develop models, which predict the correct environmental forces and response. This article builds on the model theory presented in Strand and Faltinsen (2019) on the linear wave loads on a 2D closed flexible fish cage. A modelling error has been found in Strand and Faltinsen (2019). The consequence is that the computed results change, particularly for low frequencies. However, all the main conclusions hold, more details are given in Section 2.1. This paper extends the model, including bending in the structural model to be able to handle semi-flexible structures where bending stiffness is significant. The structural model is now a half circular curved flexible 2D beam, including the effect of bending.

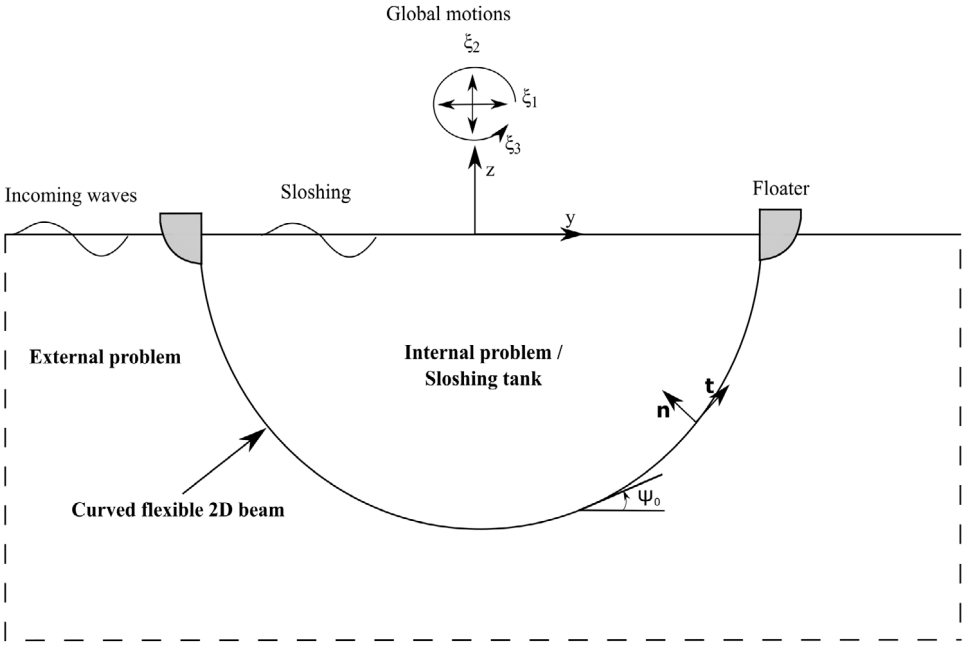

Fig. 1. Illustration of the 2D semi-flexible closed fish cage in waves.

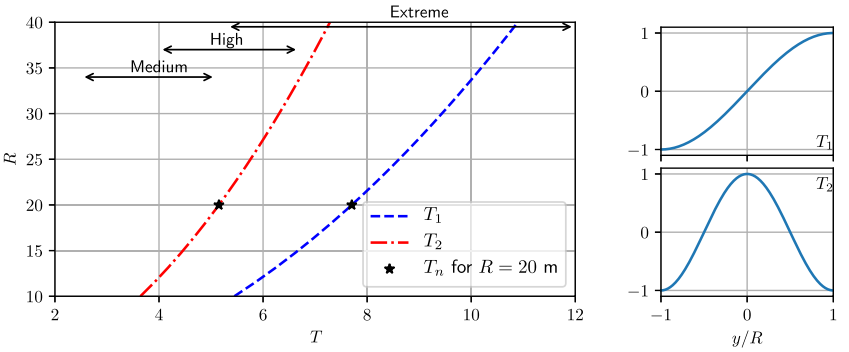

Fig. 2. Left: The two lowest natural sloshing periods related to cage radius R. Medium, high and extreme relates to the degree of wave exposure of the aquaculture cage-, defined in the Norwegian standard NS9415, see Table 1. The reference cage used in the case analysed in the results has $R = 20$ m. Right: Illustration of the free-surface shape of the two sloshing modes connected to the given sloshing periods versus y/R where y is defined in Fig. 1.

Table 1
Norwegian aquaculture site classification scheme for waves from NS9415 (2009). H_s is significant wave height and T_p is peak period of the wave spectrum.

Degree of Exposure	Small	Moderate	Medium	High	Extreme
H_s (m)	0.0–0.5	0.5–1.0	1.0–2.0	2.0–3.0	>3.0
T_p (s)	0.0–2.0	1.6–3.2	2.5–5.1	4.0–6.7	5.3–18.0

Structurally this is in the coupling field between membrane theory and thin plate theory and inspiration has been drawn from the analysis of curved floating bridges published in Li and Ren (2018) and Yang and Kuo (1987). The goal is that the theory given in the present article is consistent with the previous work on closed flexible fish cages. Our formulations are based on a linear perturbation about the static mean position of the structure. Potential flow of incompressible water is assumed. The main emphasis in Strand and Faltinsen (2019) was on cage motions, deformations and internal sloshing amplitudes. For a significantly more rigid cage, negligible changes compared to a rigid structure is expected in the rigid body motions. The beam model is the best solution in 2D. If the cage had been modelled in 3D a curved plate theory approach with membrane effects should have been used.

One major concern for the structural stresses of a closed cage is the effect of sloshing. Sloshing is internal wave motion inside the cage and have multiple resonance periods. The natural sloshing periods depend on the size, geometry and the flexibility of the cage. Typical industry concept cage geometries are either ellipsoidal, rectangular or upright cylinders. The excitation frequency of the sloshing is directly related to the wave period. The possible wave periods at an aquaculture location is dependent on the degree of wave exposure of the cage. Traditionally the aquaculture net-cages in Norway have been quite sheltered. The wave periods and wave heights encountered in sheltered areas are significantly smaller than in the North Sea. The degree of wave exposure of an aquaculture fish farm is classified in a range from small to extreme as given in Table 1. In Fig. 2 the first two sloshing periods T_1 and T_2 for a 2D half circular rigid cage is plotted versus varying cage radius R along with a visualisation of how the first two sloshing modes appear. For a 2D semi-circular geometry, the sloshing period increases for increasing radius. For cage radi smaller than $R = 20$ m the sloshing period can be excited within a medium exposure. The radius of the reference cage is marked in Fig. 2 for comparison. The second sloshing period of the reference cage will correspond to a high degree of exposure of the cage. There exist sloshing periods in the same frequency range for 3D structures also. These sloshing periods will also increase with increasing radius as the presented 2D sloshing periods.

For floating large volume offshore structures second order slowly varying and mean wave forces in a stochastic sea have great importance in the design of the mooring system. These effects will not be considered in the present analysis. Since the semi-flexible closed cage causes non-negligible far-field waves, mean and slowly varying horizontal wave forces are expected to matter also for the design of the mooring system of the semi-flexible closed cages. However, the mooring system of a semi-flexible closed cage is not modelled. Ambient current and internal structures such as pumps and pipes are neglected and would require that viscous flow is considered in a rational hydrodynamic model. It is possible and also plausible that location of the internal free surface deviates from the external free surface, as was the case for the closed flexible fish cage analysed in Strand and Faltinsen (2019). In the present work, the internal and external free surfaces are equal. Due to operational considerations, it is also plausible with different internal and external water densities; this is not considered in the present article. There are in reality several nearby cages, which means that multiple body–wave interactions matters.

Standard procedure in the analysis of the structural stresses in ships and offshore structures is to consider the structure deformation as quasi-static, meaning that the inertia and hydrodynamic effects of the structural deformations can be neglected. Is it a valid and conservative assumption to assume that the stresses in a semi-flexible fish cages can be computed with a quasi-static analysis? Alternatively, is it necessary with a complete hydroelastic analysis to find the correct stresses in the structure? Will the stresses be affected by the internal sloshing in the cage? When can the structure be assumed rigid in terms of stiffness? These are the questions we aim to solve in the following.

In this paper, the linear theory of a 2D semi-flexible closed cage in waves is developed and analysed to investigate the structural response of the semi-flexible closed cage in waves. First, a general overview of the problem and the frequency-domain equations of motions of the rigid body motions are presented. The theory for dynamic deformation of a 2D membrane is developed next. Then, the theory for the pressure loads on the semi-flexible closed cage is investigated, starting with the external hydrodynamic pressure forces, continuing with internal hydrodynamic pressure forces. The numerical solution of the hydrodynamic problem is outlined before the model for the structural stress calculation for both hydroelastic and quasi-static are given. Finally, the results from a 2D case study with relevant full-scale dimensions considering a half circularly shaped semi-flexible closed cage with floaters in waves are presented. At last conclusions with future suggested needed investigations are given.

2. Theory for wave-induced motions of a semi flexible closed fish cage

The 2D semi-flexible closed fish cage considered here is shaped in a half circular geometry with two floaters attached at the top (see Fig. 1). An Earth-fixed Cartesian coordinate system Oyz with origin in the mean free surface is introduced. The z-axis pointing upwards is in the centre-plane of the cage at rest. The vertical position of the free surface is the same on the inside and outside of the cage.

The wave-induced body motions contain the rigid body motions ξ_1, ξ_2 and ξ_3 in sway, heave and roll, respectively. Sway and heave are for a point that coincides with the origin of the coordinate system Oyz when the body is at rest. The motion of the cage is the sum of the structure deformations relative to the static shape and rigid body motions described by ξ_1, ξ_2 and ξ_3. It implies that the beam deformations are zero at the attachment points to the floaters. We assume small rigid body motions of the cage and small structural deformations. Then the superposition principle can be used. Potential flow of incompressible water with linear free-surface conditions are assumed. The external water has an infinite horizontal extent and constant finite water depth. The water surrounding and inside the cage introduces pressure forces on the combined structure.

2.1. Equation of motion

We start by formulating the equations of motions for the cage. The equations of rigid body motions follow from Newton's law and the equations of angular momentum. The cage consists of two floaters in the free surface. Attached to the floaters is a half circular curved beam. The floaters are assumed rigid, i.e. rigidly connected above the water line. We

must consider loads on the cage caused by the elastic deformations of the beam. These are expressed as coupled added mass and damping loads caused by the elastic deformations. We must account for both internal and external hydrodynamic loads acting on the structure. The change in hydrostatic loads due to body motions are accounted for in addition to dynamic weight considerations. Assuming steady-state oscillatory conditions, the rigid-body equations of motions of the cage becomes:

$$(m_T + a_{11})\ddot{\xi}_1 + b_{11}\dot{\xi}_1 + (a_{13} - z_G m_T)\ddot{\xi}_3 + b_{13}\dot{\xi}_3 = f_1^{exc} + f_1^{Beam}, \tag{1}$$

$$(m_T + a_{22})\ddot{\xi}_2 + b_{22}\dot{\xi}_2 + c_{22}\xi_2 = f_2^{exc} + f_2^{Beam}, \tag{2}$$

$$(I_{33} + a_{33})\ddot{\xi}_3 + b_{33}\dot{\xi}_3 + c_{33}\xi_3 + (a_{31} - z_G m_T)\ddot{\xi}_1 + b_{31}\dot{\xi}_1 = f_3^{exc} + f_3^{Beam}. \tag{3}$$

Here, m_T is the total mass of the floater and beam per metre, and I_{33} is the combined moment of inertia of the beam and floaters in roll defined as $I_{33} = \int(y^2+z^2)dm_T$. a_{jk} are 2D added mass coefficients associated with the internal and external flow, b_{kj} are 2D wave radiation damping coefficients and z_G is the vertical centre of gravity of the structure (not including internal water). The considered restoring coefficients c_{jk} in the equation of motions of the cage are due to quasi-steady change in the hydrostatic pressure and weight considerations, further described in Section 2.5. The effect of a mooring system is not considered. Furthermore, f_j^{exc} is wave excitation loads on the structure when restrained from oscillating. f_j^{Beam} are caused by the flow due to the normal beam deformations acting on the cage and can be expressed in terms of coupled added mass and damping coefficients. How to evaluate a_{jk}, b_{jk} and f_j^{exc} are described in Section 2.6.

In Strand and Faltinsen (2019), there appear restoring coefficients due to membrane forces at the attachment between the membrane and the floater. These internal loads will because of "action and reaction" be cancelled out, and should therefore not be there when we formulate the equations of the rigid body motions of the combined floater and membrane. If these terms are removed from the model, the consequence is that the computed results change, particularly for low frequencies. However, all the main conclusions hold.

2.2. Beam structure

To analyse the deformations and stresses a structural model is needed. A linear structural model of the dynamic deformations of a curved beam is developed and described below. The structural equations are based on Strand and Faltinsen (2019) and further extended to allow for bending. For the development of the equations, the reader is referred to Strand and Faltinsen (2019). The structural modelling is based on a curved beam, and the effect of bending is included as described in Li and Ren (2018) and Yang and Kuo (1987).

In the presented equations we make a perturbation of the static curved beam equations about the static solution such that

$$\begin{aligned} \psi(s,t) &= \psi_0(s) + \hat{\psi}(s,t) \\ T(s,t) &= T_0(s) + \tau(s,t) = T_0(s) + EA\hat{e}(s,t), \\ \Delta p(s,t) &= \Delta p_0 + \Delta\hat{p}(s,t). \end{aligned} \tag{4}$$

Here, the static tension T_0 is a static beam tension per unit length in the perpendicular x-direction. ψ_0 is the static angle defined in Fig. 1. $\tau = EA\hat{e}$ is the dynamic tension, E is the elasticity module, A is the area per metre (the thickness) of the beam, $\hat{e}$ is the dynamic strain following from the linear relation between strain and tension according to Hooke's law and $\hat{\psi}$ is the dynamic angle defined in a similar way as ψ_0. Δp_0 is the static pressure difference and $\Delta\hat{p}$ the dynamic pressure difference across the beam. s is the curvilinear coordinate along the beam, starting from $\psi_0 = 0$. Linear compatibility relations between the tangential and normal deformations (u, v), the dynamic strain $\hat{e}$ and the dynamic angle $\hat{\psi}$ exist (e.g. Ventsel, 2001):

$$\hat{e} = \frac{\partial u}{\partial s} - v\frac{\partial \psi_0}{\partial s}, \tag{5}$$

$$\hat{\psi} = \frac{\partial v}{\partial s} + u\frac{\partial \psi_0}{\partial s}. \tag{6}$$

The static tension T_0 is known from a static pressure analysis in calm water. For the given half circular configuration only loaded by the weight of the beam in water, an analytical expression exists for the static tension in the beam. The analytical expression for the static tension is developed based on the cable line equations by Faltinsen (1990, 258-261) assuming a half circular given geometry. The expression for the static tension T_0 is:

$$T_0 = RAg\frac{\pi}{2}(\rho_s - \rho_w) - RAg\rho_s\cos 2(\psi_0 + \pi/2) = T_0^c + T_0^a(\psi_0), \tag{7}$$

where ρ_s is the density of the structural material and ρ_w is the density of water. T_0 is divided in one constant part T_0^c and one angle dependent part $T_0^a(\psi_0)$.

We assume steady state oscillations and write the tangential deformations as $u(\psi,t) = u(\psi)e^{i\omega t}$ and the normal deformations as $v(\psi,t) = v(\psi)e^{i\omega t}$, where $i^2 = -1$. It implies that $u(\psi,t)$ and $v(\psi,t)$ are complex variables and that it

is the real parts of $u(\psi,t)\exp(i\omega t)$ and $v(\psi,t)\exp(i\omega t)$ that have physical meaning. The equation system for the normal (v) and tangential (u) deformations is:

$$-\omega^2 m_B v = -\frac{EI_y}{R^4}\left(\frac{d^4v}{d\psi^4}+2\frac{d^2v}{d\psi^2}+v\right)+\frac{T_0}{R^2}\left(\frac{d^2v}{d\psi^2}+\frac{du}{d\psi}\right)+\frac{EA}{R^2}\left(\frac{du}{d\psi}-v\right)-\Delta\hat{p}, \tag{8}$$

$$-\omega^2 m_B u = \frac{EA}{R^2}\left(\frac{d^2u}{d\psi^2}-\frac{dv}{d\psi}\right)-\frac{T_0^c}{R^2}\left(\frac{dv}{d\psi}+u\right). \tag{9}$$

Here, $I_y = 0.5\pi AR^2$ is the moment of inertia about the beams centreline assuming a thin beam. For a half circular geometry, the static curvature is constant, then $\frac{d\psi_0}{ds}=\frac{1}{R}$. It should be noted that when $R\to\infty$ the effect of curvature in (8) reduces to the known relations for a straight beam. In the given equations it have been used that $\frac{1}{R}\frac{dT_0}{d\psi}=m_B g\sin\psi_0$. The hydrodynamic pressure difference $\Delta\hat{p}$ in (8) depends on v, the rigid body motions as well as the incident waves and its diffraction (scattering) by the cage. Details are given in Section 2.6.

2.3. Modal representation of the beam's deformation

We will solve (8) and (9) by a modal method. The curved beam is attached to the floater at both ends. We assume a rigid floater and therefore require zero motion at the attachment point between the floater and the beam. In addition we require that the floaters do not rotate locally. This means that there cannot be any moment at the attachment point, which means a simply supported beam. The boundary conditions are then $v(\pm\frac{\pi}{2})=\frac{d^2v}{d\psi^2}(\pm\frac{\pi}{2})=u(\pm\frac{\pi}{2})=0$: The modal representation must be complete in a mathematical sense. A complete Fourier series (modal) representations of v and u that satisfy the boundary conditions with continuity of deformation at the attachment point are:

$$v = \Re\Big(\sum_{j=4}^{\infty}\xi_j V_j(\psi_0)e^{i\omega t}\Big)=\Re\Big(\sum_{j=4}^{\infty}\xi_j\sin((j-3)(\psi_0+\pi/2))e^{i\omega t}\Big) \tag{10}$$

$$u = \Re\Big(\sum_{n=1}^{\infty}\mu_n U_n(\psi_0)e^{i\omega t}\Big)=\Re\Big(\sum_{n=1}^{\infty}\mu_n\sin(n(\psi_0+\pi/2))e^{i\omega t}\Big) \tag{11}$$

where $\Re$ means the real part and ξ_j for $j>3$ and μ_n are the generalised complex structural mode amplitudes in normal and tangential direction, respectively. In the following text we will omit the symbol $\Re$ and imply implicitly that we mean the real part of a complex expression involving the complex time dependence.

The equations for the structural deformations of the beam by (8) and (9) combined with (10) and (11), multiplied with the modes and integrated along the beam length S_B, give a representation of the dynamics of the beam. $V_j(\psi_0)$ is written as V_j and $U_j(\psi_0)$ is written as U_j.

$$-\int_{-\frac{\pi}{2}}^{\frac{\pi}{2}}\omega^2 m_B v V_j R d\psi = \int_{-\frac{\pi}{2}}^{\frac{\pi}{2}}\left(-\frac{EI_y}{R^4}\left(\frac{d^4v}{d\psi^4}+2\frac{d^2v}{d\psi^2}+v\right)+\frac{T_0}{R^2}\left(\frac{d^2v}{d\psi^2}+\frac{du}{d\psi}\right)+\frac{EA}{R^2}\left(\frac{du}{d\psi}-v\right)-\Delta\hat{p}\right)V_j R d\psi, \tag{12}$$

$$-\int_{-\frac{\pi}{2}}^{\frac{\pi}{2}}\omega^2 m_B u U_j R d\psi = \int_{-\frac{\pi}{2}}^{\frac{\pi}{2}}\left(\frac{EA}{R^2}\left(\frac{d^2u}{d\psi^2}-\frac{dv}{d\psi}\right)-\frac{T_0^c}{R^2}\left(\frac{dv}{d\psi}+u\right)\right)U_j R d\psi. \tag{13}$$

We will use that the modes are orthogonal to each other.

2.4. Coupled system equations for the cage

The rigid body equation of motion given by (1)–(3) and the equations for the structural deformations of the beam by (12) and (13), together give a representation of the dynamics of the cage. In $\boldsymbol{\xi}=\{\xi_1,\xi_2,\xi_3,\xi_4....\}$, the first three terms are the rigid body motions, then the normal structural deformation modes follow. The beam influences the rigid body motion through the hydrodynamic coupling terms between rigid body motions and the structural normal deformation modes.

The coupled equation system can be expressed as:

$$\sum_{j=1}^{\infty}\left(-\omega^2(m_{ij}^{\xi}+a_{ij})+i\omega b_{ij}+c_{ij}^{M\xi}\right)\xi_j+\sum_{n=1}^{\infty}c_{in}^{M\xi\mu}\mu_n=f_i^{exc}\ \text{for}\ i=1....\infty \tag{14}$$

$$\sum_{j=1}^{\infty}c_{kj}^{M\mu\xi}\xi_n+\sum_{n=1}^{\infty}\left(-\omega^2 m_{kn}^{\mu}+c_{kn}^{M\mu}\right)\mu_n=0\ \text{for}\ k=1....\infty \tag{15}$$

Here, the non-zero m_{ij}^{ξ} for $i,j<4$ follow from (1)–(3) and are $m_{11}^{\xi}=m_{22}^{\xi}=m_T$, $m_{33}^{\xi}=I_{33}$ and $m_{13}^{\xi}=m_{31}^{\xi}=-z_G m_T$. The generalised mass coefficients m_{ij}^{ξ} for $i,j>3$ associated with the normal deformation modes are given as $m_{ij}^{\xi}=$

$m_B \int_{S_s} U_i U_{(j-3)} \mathrm{R}\mathrm{d}\psi$. The generalised mass coefficient m^{μ}_{kn} associated with the tangential deformation modes are given as $m^{\mu}_{kn} = m_B \int_{S_s} U_k U_n \mathrm{d}s$. Expressions for the structural stiffness coefficients $c^{M\xi}_{ij}$, $c^{M\mu}_{kn}$, $c^{M\xi\mu}_{in}$ and $c^{M\mu\xi}_{kj}$, for $i, j > 3$ are given as

$$c^{M\xi}_{mj} = \int_{-\pi/2}^{\pi/2} \left(\frac{EI_y}{R^4} \left(\frac{d^4 V_m}{d\psi^4} + 2\frac{d^2 V_m}{d\psi^2} + V_m \right) - \frac{T_0}{R^2} \frac{d^2 V_m}{d\psi^2} + \frac{EA}{R^2} V_m \right) V_{(j-3)} \mathrm{R}\mathrm{d}\psi \text{ for } j, m > 3, \tag{16}$$

$$c^{M\xi\mu}_{mj} = -\int_{-\pi/2}^{\pi/2} \left(\frac{T_0}{R^2} + \frac{EA}{R^2} \right) \frac{dU_m}{d\psi} V_{(j-3)} \mathrm{R}\mathrm{d}\psi \text{ for } j, m > 3, \tag{17}$$

$$c^{M\mu\xi}_{jm} = \int_{-\pi/2}^{\pi/2} \left(\frac{T^c_0}{R^2} + \frac{EA}{R^2} \right) \frac{dV_j}{d\psi} U_m \mathrm{R}\mathrm{d}\psi \tag{18}$$

$$c^{M\mu}_{jm} = \int_{-\pi/2}^{\pi/2} \left(-\frac{EA}{R^2} \frac{d^2 U_j}{d\psi^2} + \frac{T^c_0}{R^2} U_j \right) U_m \mathrm{R}\mathrm{d}\psi. \tag{19}$$

a_{ij} are the total generalised added mass coefficients with contributions from the internal and external added mass and b_{ij} are the generalised wave radiation damping coefficients from the external problem. Furthermore, $c^{M\xi}_{ij}$ for $j, i < 4$ are the generalised hydrostatic restoring coefficients. The non-zero coefficients are $c^{M\xi}_{22}$, $c^{M\xi}_{33}$ (see (20) and (21)) and $c^{M\xi}_{4,2}$ (see (20)), described in Section 2.5. f^{exc}_i are the generalised wave excitation forces (see (29)). The evaluation of the restoring coefficients will now be described in the following section.

2.5. Restoring forces and moments

If the hydrostatic pressure is integrated over the instantaneous position of the structure, it will contribute to restoring forces and moments. The change of hydrostatic pressure does not contribute to any restoring in sway. The only restoring in sway (ξ_1) would come from a mooring system. Since heave (ξ_2) causes the internal water to move vertically as a rigid body, heave does not cause change in the internal hydrostatic pressure loading. When we consider roll, there are important contributions from the internal water (Faltinsen and Timokha, 2009, page 79) following by considering the internal free surface to be horizontal. The restoring coefficient in heave (c_{22}) is

$$c_{22} = \rho_w g A_w. \tag{20}$$

The restoring coefficient in roll (c_{33}) by considering both internal and external contributions is given by

$$c_{33} = -m_T g z_G + \rho_w g \left(\nabla z_B + \int_{A_w} y^2 dy - \overbrace{\frac{2}{3}R^3 + \int_{Q_0^{(i)}} z dQ}^{\text{Tank correction terms}} \right). \tag{21}$$

When defining some of the variables in (20) and (21), we refer to a fictitious rigid body including the floaters, the beam and the water inside. Then, A_w is the waterplane area of the fictitious body, defined in 2D as $A_w = 2(R + R_F)$. g is the gravitational acceleration. ∇ is the displaced volume of water of the fictitious body per unit length; z_G is the z-coordinate of the combined centre of gravity of the floaters and beam of the cage. z_B is the $z-$ coordinate of the centre of buoyancy of the fictitious body, $Q_o^{(i)}$ is the internal water domain inside the cage.

The change in the hydrostatic pressure due to a heave motion integrated over the instantaneous body surface will give a hydrostatic restoring force for the first normal structural deformation mode. Due to orthogonality between the normal vector of heave and the normal vector of the normal deformation modes the hydrostatic pressure due to a heave motion will only effect the first normal structural mode.

$$c_{4,2} = \rho_w g \int_{S_B} n_z U_1(\psi_0) \mathrm{d}s = \rho_w g R \frac{\pi}{2}. \tag{22}$$

This term was not included in Strand and Faltinsen (2019). The effect of the hydrostatic pressure change due to a roll motion will not result in restoring forces on the normal structural modes, since the static pressure change inside and outside the cage will cancel each other out.

The generalised pressure loads due to a change in the hydrostatic pressure integrated over the instantaneous body surface will not give a hydrostatic restoring force for the normal structural deformation modes, if we assume that there is no density difference between the inside and outside water, see Strand and Faltinsen (2019). Several papers have studied the effect of hydrostatic restoring loads for elastic bodies; (Malenica et al., 2015, 2009; Senjanovic et al., 2008; Newman, 1994). The given result deviates from these studies. Common for all of the cited papers is that they define the structural modes in a Cartesian *Oxyz* coordinate system. The alternative structural representation complicates the calculations and leads to other terms. Senjanovic et al. (2008) and Newman (1994) only considered the restoring from the hydrostatic pressure on the external body, and did not account for hydrostatic pressure from any internal liquid. Malenica et al. (2015, 2009) considers hydrostatic pressure in both an internal and an external domain, but have a different free surface condition for the internal domain, leading to a restoring term from the rise of the free surface, which is included in the internal added mass expressions.

The evaluation of the generalised hydrodynamic pressure loads will now be described in the following section.

2.6. Hydrodynamic pressure loads

The pressure loads are divided into external and internal pressure loads. We will start by looking at the external pressure loads. The method for calculating the external and internal pressure loads are equal to the one used in Strand and Faltinsen (2019). It is given here in a slightly shorter version for consistency.

2.6.1. Generalised hydrodynamic external pressure loads

To find the total dynamic pressure difference on the cage we start by finding the external flow and resulting generalised pressure loads. We consider a 2D semi-flexible closed fish cage in incident regular waves of amplitude ζ_a, with wavenumber k and frequency ω at constant depth h in steady state oscillatory conditions. The wave steepness is small, and linear potential flow theory of incompressible water is assumed. It implies that the flow separation is neglected and that viscous flow is concentrated in thin body boundary layers not affecting the potential flow. For linear waves propagating in the y- direction, Faltinsen (1990) gives the velocity potential for incident waves at finite constant depth h as $\phi_0 = \frac{g\zeta_a}{\omega}\frac{\cosh k(z+h)}{\cosh kh}e^{(i\omega t - iky)}$, with the dispersion relation $\frac{\omega^2}{g} = k\tanh kh$. The presence of the body modifies the flow field in terms of a linear diffraction velocity potential ϕ_d and radiation velocity potentials $\phi_j^{(e)}$ associated with the body motions. The total external velocity potential Φ_e is given as:

$$\Phi_e = \phi_0 + \phi_d + \sum_{j=1}^{\infty}\phi_j^{(e)}\xi_j. \tag{23}$$

Here $j = 1, 2, 3$ represent the rigid body motions in sway, heave and roll, and $j = 4..\infty$ represent the normal deformation modes of the beam. The tangential deformation modes cannot cause flow within linear potential flow theory.

The boundary value problem satisfies the Laplace equation, the combined kinematic and dynamic free surface condition and no flow through the bottom at z = −h. Furthermore, a radiation condition ensures outgoing far-field waves caused by the body. The body boundary condition for the diffraction potential is:

$$\frac{\partial\phi_d}{\partial n} = -\frac{\partial\phi_0}{\partial n} \text{ on } S_s^{(e)}, \tag{24}$$

where $S_s^{(e)} = S_B^{(e)} + S_{Fl}^{(e)}$ and is the mean wetted external surface of the total structure. $S_B^{(e)}$ and $S_{Fl}^{(e)}$ are the mean wetted external beam surface and floater surface, respectively. $\frac{\partial}{\partial n}$ denotes the normal derivative to the mean wetted external body surface. The corresponding normal vector $\vec{n}$ has positive direction into the external water. Its components along the $y-$ and $z-$ axes are denoted n_y and n_z, respectively. The body boundary conditions for the radiation problems are:

$$\frac{\partial\phi_j^{(e)}}{\partial n} = i\omega n_j^{(e)} \text{ on } S_s^{(e)}. \tag{25}$$

Here $j = 1, 2, 3$ represent the rigid body motions in sway, heave and roll. It follows that

$$n_j^{(e)} = \begin{cases} n_y & \text{for } j = 1 \\ n_z & \text{for } j = 2 \\ yn_z - zn_y & \text{for } j = 3. \end{cases} \tag{26}$$

Furthermore, $j = 4..\infty$ are the prescribed normal deformation motions. It implies for $j \geq 4$ that

$$n_j^{(e)} = \begin{cases} U_{j-3}(\psi_0) & \text{on } S_B^{(e)} \\ 0 & \text{on } S_{Fl}^{(e)}. \end{cases} \tag{27}$$

Generalised added mass and damping terms for the external flow problem follows from properly integrating the time derivative of $\phi_j^{(e)}$, originating from the linear dynamic pressure part $-\rho_w\partial\Phi_e/\partial t$ in Bernoulli's equation. The expressions are given by

$$i\omega\rho_w\int_{S_s^{(e)}}\phi_j^{(e)}n_k^{(e)}\xi_j ds = \left(\omega^2 a_{jk}^{(e)}(\omega) - i\omega b_{jk}^{(e)}(\omega)\right)\xi_j \tag{28}$$

where $a_{kj}^{(e)}$ and $b_{kj}^{(e)}$ are the external 2D added mass and damping contribution in the k direction, due to a motion in the j direction.

The generalised wave excitation loads f_k^{exc} are

$$i\omega\rho_w\int_{S_s^{(e)}}(\phi_0 + \phi_d)n_k^{(e)} ds = f_k^{exc}(\omega) \tag{29}$$

Relations between the damping and the far-field wave amplitude, and between the generalised wave excitation force components and damping, together with a symmetry relation based on Green's second identity were used to verify the correctness of the numerical code. Results from these tests can be found in Strand (2018).

2.6.2. Internal water pressure loads

We assume linear potential flow theory of an incompressible liquid for the internal domain. For the internal flow, it is most convenient to operate in a tank-fixed reference system. The coordinate axes of the tank-fixed coordinate system at tank rest, are parallel to the axes of the global body-fixed coordinate system. Translatory motions are defined along tank-fixed axes and related to the origin of the internal tank-fixed coordinate system. At rest, the origin of the tank-fixed reference system is placed at the origin of the global inertial coordinate system, see Fig. 3. Since we assume small motions and deformations, origins of the inertial reference system and tank-fixed reference system at rest are collocated. Due to the assumptions of small motions and deformations, the difference in the representation of the rigid body motions and membrane deformations are the same when considering the internal and external problems. In the tank-fixed coordinate system, Bernoulli's equation in its original form must be modified to an accelerated coordinate system (Faltinsen and Timokha, 2009, page 47). As long as we operate with a linear system the linearised version of the pressure, or more precisely excess pressure relative to atmospheric pressure will be

$$p = -\rho_w \frac{\partial \Phi_i}{\partial t} - \rho_w g \xi_3 y - \rho_w g z, \tag{30}$$

with Φ_i as the internal velocity potential. The equation is consistent with that the excess pressure is zero at $z = 0$ when the tank is at rest.

The internal velocity potential Φ_i can be expressed as

$$\Phi_i = \sum_{j=1}^{\infty} \phi_j^{(i)} \xi_j. \tag{31}$$

The velocity potential $\phi_j^{(i)}$ satisfies

$$\frac{\partial^2 \phi_j^{(i)}}{\partial y^2} + \frac{\partial^2 \phi_j^{(i)}}{\partial z^2} = 0 \text{ in } Q_0^{(i)}, \tag{32}$$

$$\frac{\partial \phi_j^{(i)}}{\partial n} = \mathrm{i}\omega n_j^{(i)} \text{ on } S_s^{(i)}. \tag{33}$$

Here $Q_0^{(i)}$ is the mean internal liquid domain, $S_s^{(i)} = S_{Fl}^{(i)} + S_B^{(i)}$ is the total internal mean wetted surface, where $S_{Fl}^{(i)}$ is the mean internal wetted floater surface and $S_B^{(i)}$ is the internal wetted surface of the beam.

The internal normal vector $\vec{n}^{(i)} = (n_y^{(i)}, n_z^{(i)})$ has positive direction into the internal water. We define similarly as for the external problem

$$n_j^{(i)} = \begin{cases} n_y^{(i)} & \text{for } j = 1 \\ n_z^{(i)} & \text{for } j = 2 \\ y n_z^{(i)} - z n_y^{(i)} & \text{for } j = 3, \end{cases} \tag{34}$$

and introduce for the prescribed normal deformation modes for $j = 4..$ that

$$n_j^{(i)} = \begin{cases} -U_{j-3}(\psi_0) & \text{on } S_B^{(i)} \\ 0 & \text{on } S_{Fl}^{(i)}. \end{cases} \tag{35}$$

At the free surface, we linearise (30) at the internal free surface $z - \zeta_i = 0$, where ζ^i describes the internal wave elevation relative to the movable, tank-fixed coordinate system. We then arrive at the linearised dynamic free surface conditions in the body fixed coordinate system:

$$\frac{\partial \Phi_i}{\partial t}|_{\Sigma_0^{(i)}} + y g \xi_3 + g \zeta^i = 0. \tag{36}$$

Here, $\Sigma_0^{(i)}$ is the mean free surface inside the tank. The kinematic linearised free surface conditions is (Faltinsen and Timokha, 2009, page 198):

$$\frac{\partial \Phi_i}{\partial z} - \dot{\xi}_2 - y\dot{\xi}_3 - \frac{\partial \zeta^i}{\partial t} = 0 \tag{37}$$

Eq. (37) is not the same as in an Earth-fixed coordinate system. Changes had to be made to include the inertial terms due to the rigid body motions and due to the effect of the gravitational acceleration in the body-fixed coordinate system. In addition, conservation of liquid mass

$$\int_{\Sigma_0^{(i)}} \zeta^i dy = \int_{S_s^{(i)}} \sum_{j \geq 4} n_j^{(i)} \xi_j \mathrm{d}s, \tag{38}$$

must be satisfied.

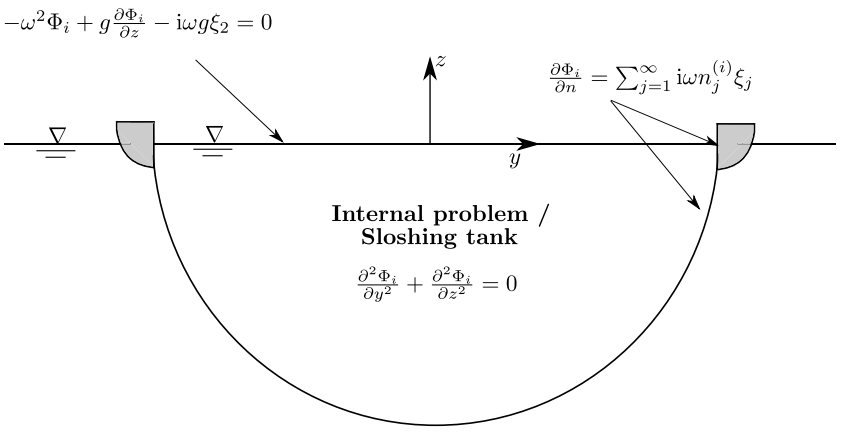

Fig. 3. Boundary conditions for the internal problem of a two-dimensional half circular closed flexible fish cage with floaters in the frequency domain.

If $\int_{S_M^{(i)}} n_j^{(i)}\xi_j \mathrm{d}s \neq 0$ for $j \geq 4$ for a given non-zero ξ_j, a constant change in the free surface exist, meaning that the mean free surface will not be located at $z = 0$. By combining (37) with the time derivative of (36) in the frequency domain, we get the linearised free surface condition

$$-\omega^2\Phi_i + g\frac{\partial\Phi_i}{\partial z} - \mathrm{i}\omega g\xi_2 = 0. \tag{39}$$

As a consequence of properly integrating the time derivative part of the pressure as given by Bernoulli's equation related to the tank-fixed coordinate system, we obtain the following added mass coefficients $a_{jk}^{(i)}$

$$\mathrm{i}\rho_w\omega \int_{S_s^{(i)}} \phi_j^{(i)} n_k \xi_j \mathrm{d}s = \omega^2 a_{jk}^{(i)}(\omega)\xi_j \tag{40}$$

where $a_{jk}^{(i)}$ is the internal 2D added mass contribution in k direction, due to a motion in j direction. There are no damping coefficients according to potential flow theory for the interior problem. The hydrodynamic damping coefficients associated with viscous boundary layer at the wetted body surface will be neglected. However, this damping is in reality small (Faltinsen and Timokha, 2009, page 377).

Symmetry of coefficients can also be used to verify the internal added mass coefficients, by using Green's second identity as was done for the external problem. Due to the free surface condition for heave, we will not have that $a_{jk}^{(i)} = a_{kj}^{(i)}$ for coupling terms between heave and the normal deformation modes.

The internal relative wave elevation ζ^i follows from the dynamic free-surface condition (36):

$$\zeta^i = -\frac{i\omega}{g}\sum_{j=1}^{\infty} \phi_j^{(i)}\xi_j|_{\Sigma_0^{(i)}} - y\xi_3. \tag{41}$$

2.6.3. Numerical flow method

A numerical solution using the Harmonic Polynomial Cell (HPC) method has been implemented to find the hydrodynamic pressure loads on the cage. The HPC method is a field method initially described by Shao and Faltinsen (2014a,b) to solve the Laplace equation with boundary conditions for an unknown velocity potential together with initial conditions in the time domain and periodicity condition in the frequency domain. In the HPC method, the local expression of the velocity potential within a cell uses harmonic polynomials. Hence, the governing equation is satisfied naturally. The connectivity between different cells is built by overlapping the local expressions. A key feature of the HPC method is in using higher-order local expressions satisfying Laplace equation, which means that we can expect better accuracy than for many other low order field and boundary integral formulations presently used. Moreover, the HPC method operates with a sparse coefficient matrix, so that many existing numerical matrix solvers can solve the associated problem efficiently. For more description of the HPC method see Shao and Faltinsen (2014a,b) and Ma et al. (2017).

For the rectangular tank with a flexible wall analysed in Strand and Faltinsen (2017) the computational domain was rectangular and easily discretised with quadratic cells. Since the geometry of the cage is not rectangular, a method to account for a non-rectangular boundary must be used. Ma et al. (2017) have found that the traditionally used HPC method has the best accuracy for quadratic grid cells and that severe stretching or distortion of the cells should be avoided. Inspired by Hanssen et al. (2015), who successfully implemented an immersed boundary method (IBM) for a moving body, we use a fixed Cartesian quadratic grid, with an immersed boundary method to capture the boundary.

Two domains are used, one internal domain and one external domain. Inspired by Hanssen et al. (2017) ghost nodes inside (for the external problem) and outside (for the internal problem) the body are applied to reconstruct the velocity at the immersed boundary. The placement of nodes is equivalent to as done for the free surface in Hanssen et al. (2017). Illustrations can be found there. The body-boundary condition on immersed boundaries are projected onto the surrounding ghost nodes. The applied code uses one layer of ghost nodes and uses the harmonic polynomials of the HPC method to interpolate the coordinate of the boundary to the ghost cell as done in Hanssen et al. (2017).

The numerical HPC framework was implemented in Python. To find the immersed boundary, the Python package "Shapely" was used. Based on predefined structural input points defining the geometry, a point on the boundary inside the cell based on linear approximation between the predefined structural input points was found.

The external domain has infinite horizontal extent and constant water depth. The far field velocity potential is expressed as outgoing waves, that are patched with the solution expressed by the HPC method near the body. According to Billingham and King (2009), the far-field velocity potential in terms of outgoing waves is a good approximation as long as $l \geq 4h$, where l is the total length of the domain.

The different examined velocity potentials caused by the body have symmetric and antisymmetric properties with respect to a symmetry line containing the z-axis. The latter fact follows from symmetry and antisymmetry properties of the generalised normal components of the mean submerged body surface $n_j^{(e)}$. $n_1^{(e)}$ and $n_3^{(e)}$ are antisymmetric while $n_2^{(e)}$ is symmetric. When $j > 3$, the odd membrane modes $((j-3) = 1, 3, 5...)$ are symmetric while the even membrane modes$((j-3) = 2, 4, 6...)$ are antisymmetric. Furthermore, the body boundary condition for the diffraction potential can be divided into symmetric and antisymmetric parts. The symmetric and antisymmetric properties allow us to only consider half the water domain. When the body boundary condition is antisymmetric, the far-field complex wave amplitude $A_j^{(+)} = -A_j^{(-)}$ and $\phi_j^{(e)} = 0$ at the symmetry line. $A^{(+)}$ and $A^{(-)}$ represent far-field complex wave amplitudes and are unknowns in solving the problem. The properties for symmetric potentials are $A_j^{(+)} = A_j^{(-)}$, and $\partial\phi_j^{(e)}/\partial y = 0$ at the symmetry line. These conditions are used as a boundary conditions at the symmetry line. Due to the symmetry and antisymmetry properties of the system it is sufficient to only consider the right part of the tank. The boundary condition on the right wall of the domain then becomes

$$\frac{\partial \phi_j^{(e)}}{\partial y} = -\mathrm{i}\omega A_j^{(+)} \frac{\cosh k(z+h)}{\sinh kh} e^{(\mathrm{i}\omega t - \mathrm{i}k\frac{l}{2})} \text{ on } y = \frac{l}{2}. \tag{42}$$

3. Calculating the structural stress and the quasi-static equations for the system

We wish to compare the stresses in the curved beam part of the structure when calculated as hydroelastic with a quasi-static approach. To consider the structure deformation as quasi-static, mean that the inertia and hydrodynamic effects of the structural deformations can be neglected. It means that one considers the structure rigid and find the resulting dynamic pressure distribution along the body. The motions of the body is found from:

$$\sum_{j=1}^{3}\left(-\omega^2(m_{ij}^{\xi} + a_{ij}) + \mathrm{i}\omega b_{ij} + c_{ij}\right)\xi_j = f_i^{exc} \text{ for } i = 1, 2, 3. \tag{43}$$

The dynamic pressure distribution following from the rigid body motion is then used in a static structural analysis. When the curved beam part of the cage is considered, the quasi-static equations (14)–(15) must be revised to the following equation system:

$$\sum_{j=4}^{\infty} c_{ij}^{M\xi}\xi_j + \sum_{n=1}^{\infty} c_{in}^{M\xi\mu}\mu_n = f_i^{exc} + \sum_{j=1}^{3}\left(\omega^2 a_{ij} - \mathrm{i}\omega b_{ij} - c_{ij}\right)\xi_j \text{ for } i = 4....\infty \tag{44}$$

$$\sum_{j=4}^{\infty} c_{kj}^{M\mu\xi}\xi_j + \sum_{n=1}^{\infty} c_{kn}^{M\mu}\mu_n = 0 \text{ for } k = 1....\infty \tag{45}$$

The right hand side of Eq. (44) is generalised pressure loads due to rigid body motions. The coupled added mass terms connected to the rigid body motions comes from integrating the pressure terms resulting from the rigid body motions.

The stresses including the bending stresses are calculated according to:

$$\sigma_1 = \frac{E}{R}\left(\frac{du}{d\psi} + v - \frac{z_L}{R}\left(\frac{d^2v}{d\psi^2} - \frac{du}{d\psi}\right)\right) \tag{46}$$

where z_L is the local height of the beam. The stress is evaluated at $z_L = A/2$ (Yang and Kuo, 1987).

4. Results

We aim to build knowledge of the structural response of the 2D semi-flexible closed fish cage in waves. A case study based on the given system description has, therefore, been conducted. Full scale 2D structural values for a plausible semi-flexible closed fish cage build in a composite material are given in Table 2. One geometry in terms of the cage radius R

Table 2
Case dimensions for a 2D semi-flexible closed fish cage with floaters. R is the radius of the semi-circular cage, A_0 is the effective cross-dimensional area per metre (the thickness) of the composite material, E_0 is the effective elasticity module of the composite material, ρ_s is the effective density of the structure, R_F is the radius of the floaters, and m_{Fl} is the mass of a floater per metre.

R	A_0	E_0	ρ_s	R_F	m_{Fl}
20 m	$10 \cdot 10^{-3}$ m	$22.4 \cdot 10^9$ Pa	2000 kg/m^3	1.5 m	2607.5 kg/m

and floater radius R_F have been used for all the analysis. The composite structure is in 3D composed of multiple layers and is stiffened, therefore an effective cross sectional area A_0, elasticity modulus E_0 and density ρ_s have been used in this 2D case. The external geometry is equivalent to the external geometry used in Strand and Faltinsen (2019) in a different scale, while the internal geometry is not equal. The cage is in static equilibrium related to weight and buoyancy. The mass of the floaters has been used to balance the structure so that the cage in equilibrium with the floaters is exactly vertical at the free surface. The wave-induced response of a semi-flexible closed fish cage with a semi-circular curved beam geometry has been analysed in the frequency domain, at finite water depth for water depth-to-radius ratio $h/R = 4.0$. We have to use a finite water depth in the HPC-code, but the water depth in practice can be considered infinite for practical wave frequencies. The used density of sea water is $\rho_w = 1025$ kg/m^3. The non-dimensional squared frequency range $0.2 \leq \omega^2 R/g \leq 5.6$ is considered, which includes wave peak periods in the weather range from moderate to extreme in NS9415 (2009) (Norwegian standard) for a semi-flexible closed fish cage with full scale radius $R = 20$ m. Furthermore, the three lowest natural sloshing frequencies for the rigid body occur in the considered frequency domain. In principle, the sloshing eigenfrequency for a flexible structure is dependent on the stiffness of the structure (Strand and Faltinsen, 2017). However, the effect is very small in the considered cases. Therefore, we have chosen to relate the results to the sloshing eigenfrequencies of a rigid structure. For the given reference case, the effect of the static tension in the model can be neglected. If the effect of overfilling or density difference is added, the tension will increase, and the effect will be more significant. No structural damping has been included in the presented analysis. The structural damping is uncertain and will be dependent on the material properties which changes for different stiffnesses.

A finite number of modes ξ_i, $i = 1...I$ and μ_k, $k = 1..K$ are considered, where I and K follow from convergence studies. I = 20 normal and K = 20 tangential modes have been used in the analysis. The external resolution of the grid is 75 nodes /R. The modes require high resolution, and it have been found that 20 nodes per modal wave length along the boundary is sufficient to reach an acceptable convergence. The internal spacial resolution is 200 nodes/R. The internal domain is much smaller (2RxR versus 16Rx4R)than the external domain, and a finer grid resolution can therefore be used without significant extra cost.

The questions we aim to answer is: Is it a valid and conservative assumption to assume that the stresses in a semi-flexible fish cages can be computed with a quasi-static analysis? Will the stresses be affected by the internal sloshing in the cage? Alternatively, is it necessary with a complete hydroelastic analysis to find the correct stresses in the structure? If a hydroelastic analysis is necessary or not, is dependent on the stiffness of the structure. For which stiffness will it be necessary with a hydroelastic analysis? The investigation of the effect of changing the stiffness has been done by varying the stiffness given by EA in the analysis. Four stiffnesses in terms of EA have been investigated, $EA/E_0A_0 = 10$ will correspond to a steel structure with the same thickness as the reference structure, $EA/E_0A_0 = 1$ is the reference composite structure, $EA/E_0A_0 = 10^{-1}$ is a softer composite structure and $EA/E_0A_0 = 10^{-2}$ is comparable to the stiffness of the fabric membrane structure analysed in Strand and Faltinsen (2019) without the extra tension due to overfilling. Since the dynamic stresses depend on the rigid body motions we start with discussing them.

4.1. Body motions

The rigid body motion response of the cage for the lowest investigated stiffness ($EA = E_0A_0 \times 10^{-2}$) is plotted together with the reference case in Fig. 4. Normal and tangential deformations for $EA = E_0A_0 \times 10^{-2}$ are plotted in Fig. 5. For the reference stiffness, the rigid-body motions of the cage are almost identical to the rigid structure motions, and the cage does not have significant deformations affecting the global rigid-body motions of the cage. However, for the smallest stiffness, the elastic deformations are significant, and the rigid body motion of the structure is affected, as was the case for the closed flexible fish cage studied in Strand and Faltinsen (2019).

When expressing the small-frequency asymptotic heave amplitude, velocity and acceleration dependent terms become higher order. The wave excitation pressure at the body has an amplitude $\rho_w g \zeta_a$ and is in phase with the incident wave amplitude at $y = 0$ The inward normal deformation of the beam is in phase with heave and causes an internal rise up of water due to conservation of water mass. The consequence is a heave force that is 180° out of phase with heave. The symmetric normal and tangential elastic modes are coupled as a consequence of the radius of curvature of the elastic beam in static conditions. Mathematical details can be found in Strand and Faltinsen (2019) when bending stiffness is neglected. When the stiffness increases the deformations decrease, and the effect of the internal rise of the free surface diminishes and we get the rigid body result that the asymptote of heave approaches one. The asymptote of sway and roll

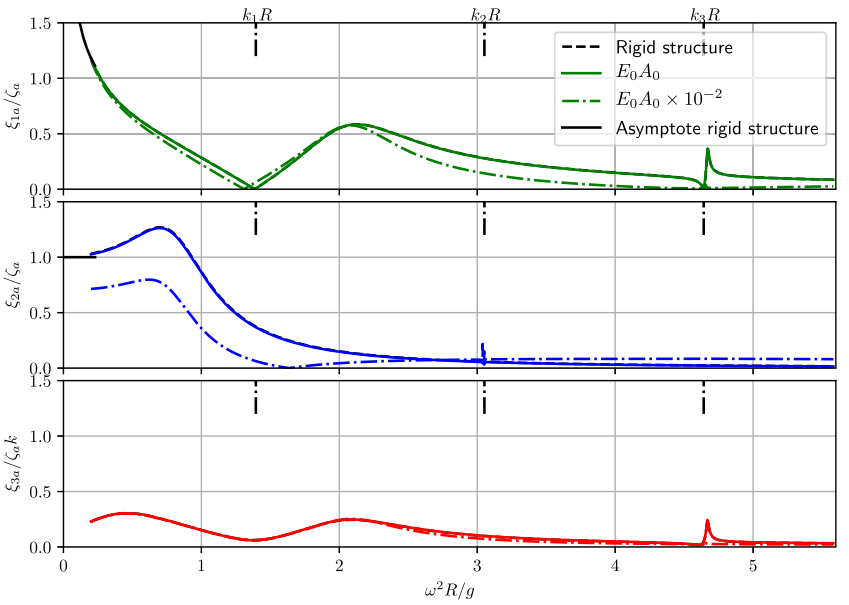

Fig. 4. Transfer functions of rigid-body motions of a semi-flexible closed fish cage for sway (top), heave(middle) and roll (bottom), with and without the effect of the deformable membrane versus non-dimensional squared frequency $\omega^2 R/g$. k_1R, k_2R and k_3R are non-dimensional squared natural sloshing frequencies for the rigid structure.

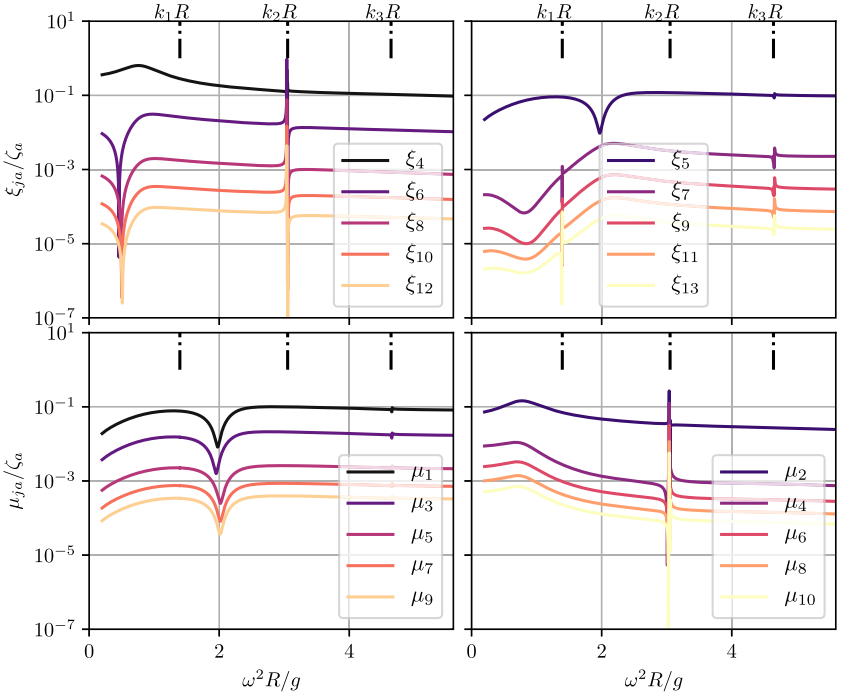

Fig. 5. Transfer functions of normal (top figures) and tangential (bottom figures) elastic modes for a semi-flexible closed fish cage versus non-dimensional squared frequency $\omega^2 R/g$, for the first 10 normal and tangential structural modes. k_1R, k_2R and k_3R are non-dimensional squared natural sloshing frequencies. $EA = A_0A_0 \times 10^{-2}$.

when $\omega \to 0$ is not affected by the stiffness of the beam. Since sway and roll is not coupled to the symmetric normal deformation modes, this is to be expected. The trough in Fig. 5 at kR around two are due to cancellations caused by coupling between the first antisymmetric mode, sway and roll, effecting the tangential modes. Similarly, the trough at kR around 0.6 are due to coupling between heave and the symmetric normal modes above the first normal structural mode.

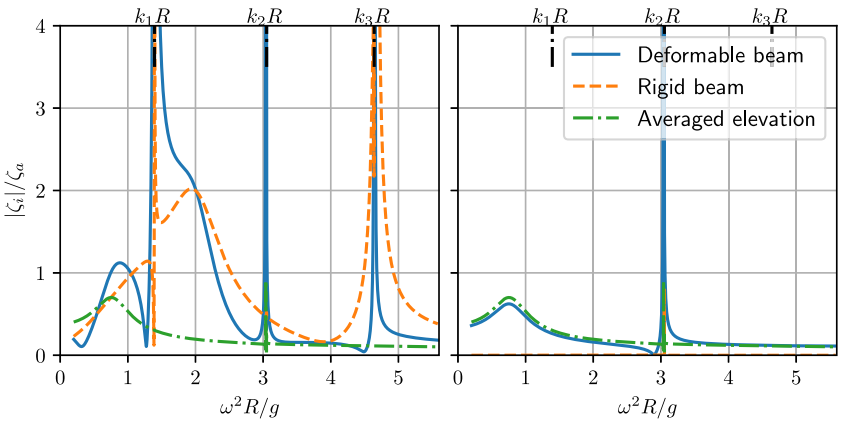

Fig. 6. Transfer functions $|\zeta_i|/\zeta$ of the internal wave amplitude at the right floater (left figure) and at the centre (right figure) of the semi-flexible closed cage versus non-dimensional squared frequency ω^2R/g for non-dimensional stiffness $EA/E_0A_0 = 10^{-2}$. The space-averaged wave amplitude calculated by Eq. (38) is also presented. k_nR are non-dimensional squared natural sloshing frequencies.

We are particularly interested in the structural response close to the sloshing frequencies. The pressure at the sloshing frequencies is theoretically infinite for sloshing in tanks with forced oscillations (Faltinsen and Timokha, 2009), while they showed that the rigid body motions of a floating rigid structure with internal tanks are either zero or finite at the antisymmetric non-dimensional sloshing frequencies k_1 and k_3. This is consistent with the results shown here. Sloshing cannot be excited by heave according to linear theory. It should be noted that the heave response from the hydroelastic analysis have a small peak response close to the second non-dimensional sloshing frequency (k_2). This response is due to an elastic response of the symmetrical normal structural modes, which experience a resonance at this frequency as can be seen in Fig. 5. This was not observed in Strand and Faltinsen (2019). However, the total stiffness in this simulated case is smaller than the total stiffness used in Strand and Faltinsen (2019), since the static tension T_0 in (8) is much smaller here. The tension is smaller because overfilling is not considered.

4.2. Internal sloshing in the cage

At the sloshing frequencies the wave elevation and the hydrodynamic pressure is theoretically infinite at k_1 and k_3 for forced oscillations of a rigid tank according to linear potential flow theory of an incompressible liquid. However, due to the external wave radiation damping there will be some energy dissipation resulting in that the internal wave elevation will be finite in our considered problem. The absolute internal wave elevation is plotted in Fig. 6 for stiffness $EA/E_0A_0 = 10^{-2}$ and a rigid cage. The numerical results for the rigid cage is consistent with the theoretical analysis given in Faltinsen and Timokha (2009). For the deformable cage we see a resonance response of the wave elevation at all the given non-dimensional squared sloshing frequencies including the second. The wave elevation response at the second sloshing frequency is caused by symmetric flexible deformations. The results indicate that the elasticity of the tank has a very small influence on the sloshing frequencies of the cage.

4.3. Transfer function of stress

We have investigated what happens with the stress in the curved beam part of the semi-flexible closed fish cage for increasing and decreasing stiffness relative to the reference composite structure. The transfer function of the stress in the curved beam is plotted in Fig. 7. $|\sigma_{max}|/\zeta_a\rho_w g$ is the maximum non-dimensional stress along the curved beam calculated at $z_L = A/2$ at a given non-dimensional frequency ω^2R/g found from a hydroelastic analysis, while $|\sigma^{qs}_{max}|/\zeta_a\rho_w g$ is the maximum non-dimensional stress found from a quasi-static analysis. We will discuss to what extent the structural stress can be considered quasi-steady according to linear frequency domain theory. Furthermore, do structural and sloshing natural frequencies cause peaks in the transfer function.

One way of qualitatively examining if a structure should be examined with a quasi-static or a hydroelastic analysis is to investigate where structural elastic frequencies are relative to the relevant wave frequency band. If the critical structural elastic natural frequencies are sufficiently high relative to the relevant wave frequencies the problem is assumed quasi-static. The structural natural frequencies increase with increasing mode number, therefore the first and second structural eigenfrequencies will be examined. The first eigenfrequency is connected to a symmetric mode, and it will not have an effect of bending, while the second eigenfrequency is connected to an antisymmetric mode and will have an effect of bending. The eigenfrequencies of the uncoupled first (ω_1) and second (ω_2) structural normal mode can be expressed as:

$$\omega_1 = \sqrt{\frac{\pi(T_0 + EA)}{R(\pi Rm_B + 2a_{44})}},\ \omega_2 = \sqrt{\frac{\pi(T_0 + EA + 9EI/R^2)}{R(\pi Rm_B + 2a_{55})}} \tag{47}$$

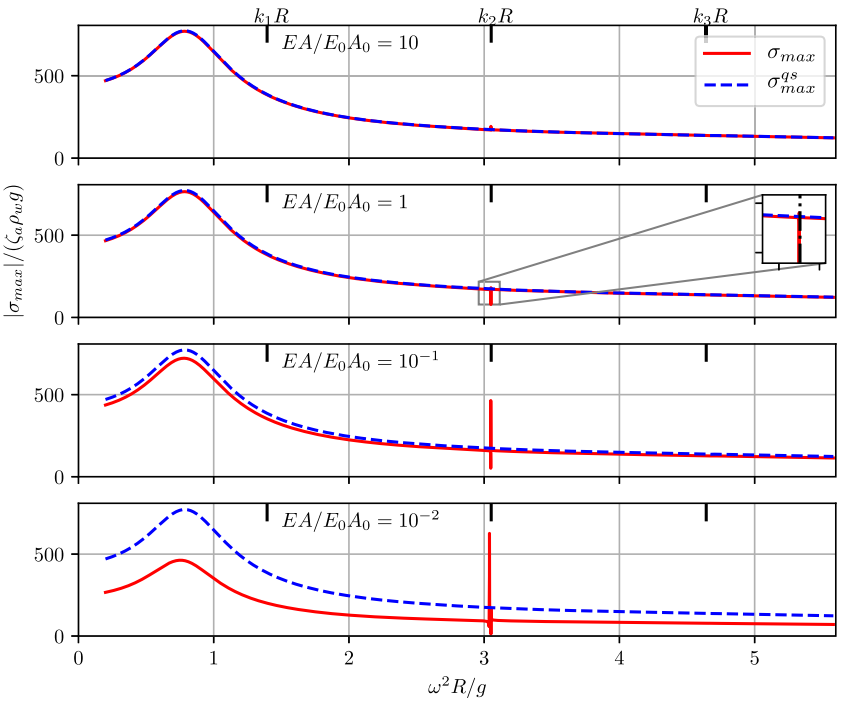

Fig. 7. Plot of transfer function of the max stress in the circular beam part of the cage for varying stiffness EA. $|\sigma_{max}|/\zeta_a\rho_w g$ is the maximum non-dimensional stress at a given non-dimensional squared frequency ω^2R/g found from a full hydroelastic analysis, and $|\sigma^{qs}_{max}|/\zeta_a\rho_w g$ is the maximum non-dimensional stress found from a quasi-static analysis. k_nR are non-dimensional squared natural sloshing frequencies.

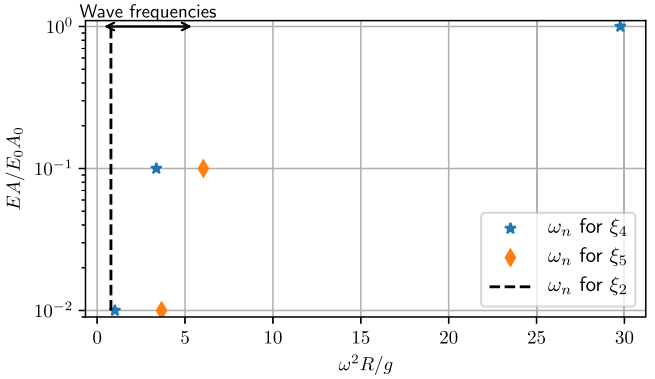

Fig. 8. Plot of the two lowest uncoupled eigenfrequencies ω_n (for ξ_4 and ξ_5) as function of non-dimensional squared frequency ω^2R/g for varying non-dimensional stiffness EA/E_0A_0. The relevant wave frequency band investigated here, is indicated on the top. The eigenfrequency of heave ξ_2 is added for reference.

For the non-dimensional frequencies above the examined range, the added mass of the structural mode a_{jj} is assumed constant and equal to the added mass of the last examined frequency ($a_{jj}(\omega_{max})$) in the estimates. The uncoupled first and second structural normal eigenfrequencies are plotted in Fig. 8. For the two lowest stiffnesses examined, the first uncoupled structural eigenfrequency is within the relevant wave frequency band, for the two higher stiffnesses the eigenfrequency is significantly higher than the relevant wave frequency band. While for the second mode only the eigenfrequency for the lowest stiffness is within the wave frequency band. The eigenfrequencies for the stiffnesses not shown are outside the given frequency range. Based on the criterion that the uncoupled eigenfrequency should be within the frequency band alone, the two highest stiffnesses could be analysed by a quasi-static approach, and the two lowest should be analysed with a hydroelastic analysis.

The system is coupled both between the normal and tangential modes and towards the rigid-body motions. Since the structural modes are coupled, it is therefore not certain that the total system will have a resonance response at the calculated uncoupled frequencies. For the lowest stiffness the normal and tangential deformations of the first ten

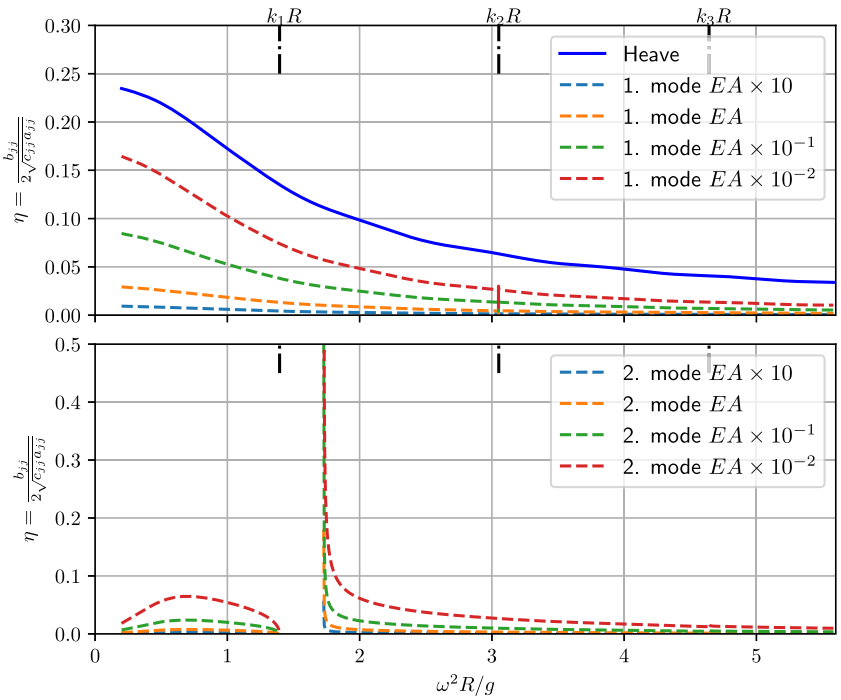

Fig. 9. Calculated uncoupled damping ratios for the first and the second normal structural mode given as $\eta = \frac{b_{jj}}{\sqrt{c_{jj}a_{jj}}}$ versus nondimensional frequency $\omega^2 R/g$ for varying nondimensional stiffness EA/E_0A_0.

modes are plotted in Fig. 5. At the calculated first eigenfrequency a small but clear top can be seen. This is close to the eigenfrequency in heave, and appears to also influence the rigid-body motion in heave as can be seen in Fig. 4. That the resonance response is small indicates that the damping level is high. The ratios η between the damping and the critical damping for the first two modes for different stiffnesses are plotted in Fig. 9. The damping level of heave is added for reference. If we look at the damping level for the first mode close to the first eigenfrequency, we see that the damping ratio η is indeed large in the relevant frequency range. At the calculated second eigenfrequency for the lowest stiffness, no response could be observed in either the rigid body motions or in the normal and tangential deformations.

From Fig. 7, we observe that the coupled hydroelastic results are in general lower than the quasi-static results. As the stiffness decreases the stresses computed by the hydroelastic model decreases simultaneously. Based on the plotted results, it can be concluded that to use the quasi-static assumption is conservative within the given frequency range, for all examined frequencies except the frequencies close to the second sloshing frequency.

There are no peaks in the stress results at the sloshing frequencies corresponding to k_1 and k_3. Since the stresses are functions of the rigid and elastic motion components, the stress results are consistent with the motion results. Close to the second non-dimensional sloshing frequency (k_2) for the examined stiffnesses, a localised peak can be observed in the coupled hydroelastic results. The stress peak is very localised in terms of frequency. The stress is dependent on the frequency resolution close to the sloshing frequency and the damping level of the relevant deformation modes at the relevant frequency. The resolution is improved close to the second sloshing frequency. However, the exact stress level at the sloshing frequency cannot be determined. The fact that the hydrodynamic pressure becomes very large at the natural sloshing frequencies do not imply that the motions and hence the stress becomes very large. This has theoretically been shown in Faltinsen and Timokha (2009) for the motions of a rigid tank. The reason for this behaviour is infinite added mass due to sloshing at the natural sloshing frequencies. If the motion system is uncoupled, this leads to zero motion response at the natural sloshing frequencies. If the motion system is coupled the behaviour of combination of coupled sloshing added mass coefficient makes finite non-zero motion response possible at the natural frequencies. Since the sloshing added mass coefficients associated with flexible normal modes are also infinite at the natural sloshing frequencies, it is plausible that the response of the flexible normal modes are finite at the natural sloshing frequencies. However, such theoretical analysis has not been performed. The second non-dimensional squared sloshing frequency k_2R is a frequency connected to a symmetric sloshing mode illustrated in Fig. 2 left part. Rigid body motions are not affected at the symmetric sloshing frequency for an assumed rigid structure, and are therefore also not visible in the stress results from the quasi-static analysis.

The structural stress is directly coupled to the normal and tangential deformation modes in (46). From Fig. 5 which is the plot of the first ten normal and tangential modes for the lowest stiffness, we can clearly see that at the second

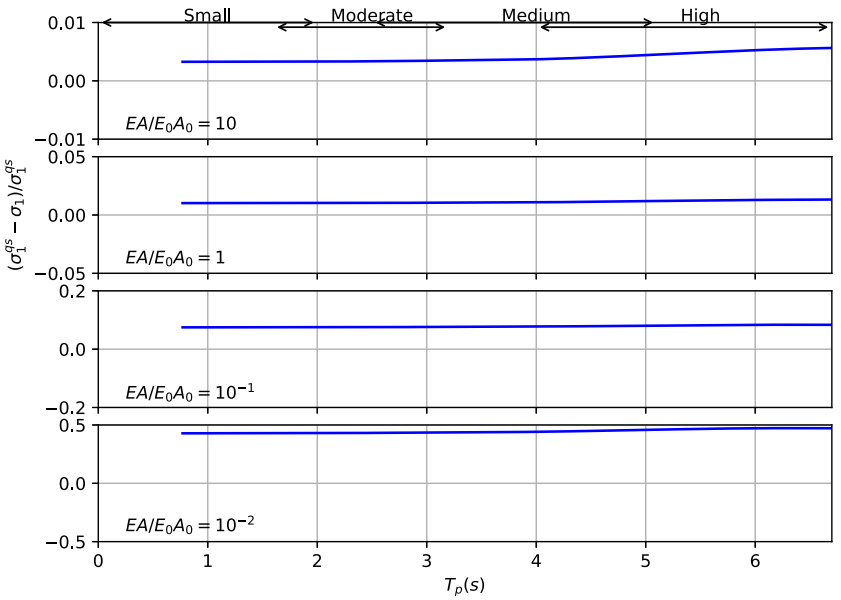

Fig. 10. The relative difference $(\sigma_1^{qs} - \sigma_1)/\sigma_1^{qs}$ of the standard deviation of the maximum dynamic stress along the beam by a quasi-steady (σ_1^{qs}) and a hydroelastic (σ_1) analysis for given exposure versus wave peak period T_p in sea states defined by a JONSWAP spectrum. The small, moderate, medium and high refers the classification related to exposure as given in NS9415 (2009).

non-dimensional squared sloshing frequency (k_1) both the normal and the tangential response are significant for the symmetric normal modes $(\xi_3, \xi_5, \xi_7...)$ and the antisymmetric tangential modes $(\mu_2, \mu_4, \mu_6...)$. This is consistent with the stress peaks at the second non-dimensional squared sloshing frequency. The effect of the first and third sloshing frequency is not evident in the stress transfer function. These two frequencies are anti-symmetric sloshing modes connected to sway and roll, the antisymmetric normal modes $(\xi_4, \xi_6, \xi_8...)$ and the symmetric tangential modes $(\mu_1, \mu_3, \mu_5...)$.

As the stiffness decreases the stresses computed by the hydroelastic model decreases, simultaneously, the deformations increase. The deformations in the hydroelastic analysis increase to a point where the deformations are significant and affect the motions of the structure (see Figs. 4 and 5) as could be seen for the closed flexible fish cage studied in Strand and Faltinsen (2019), which were a membrane structure.

4.4. Structural stresses in a sea state

The dynamic structural stresses in a sea state are dependent on both the wave height and the wave frequency. The response in irregular sea should be calculated to find the relevant stress level wave response. Then the squared stress transfer function must be multiplied with a sea state spectrum and properly integrated to find the actual effect in a given sea state. The standard deviation of the dynamic stress σ_1 for a given sea state spectrum $S(\omega)$ in long crested waves can be calculated as:

$$\sigma_1^2 = \int_0^\infty S(\omega)\left(\frac{\sigma_{max}}{\zeta_a}\right)^2 \mathrm{d}\omega. \tag{48}$$

where σ_{max}/ζ_a is the transfer function of the maximum stress along the curved beam calculated at $z_L = A/2$ based on hydroelastic analysis, and σ_1^{qs}/ζ_a can be calculated by Eq. (48) exchanging σ_{max} with σ_{max}^{qs}. The Norwegian standard (NS9415, 2009) for the design of aquaculture fish farm in the sea requires for calculation of response from irregular sea that the JONSWAP spectrum shall be used with $\gamma = 2.5$ for wind-generated seas, where γ is the spectral peakedness parameter. The JONSWAP spectrum is for limited fetch, and in the standard, it is required that a fully developed sea state is assumed. A γ-value of 2.5 is lower than for ships and offshore structures where $\gamma = 3.3$.

The JONSWAP spectrum is

$$S(\omega) = \frac{\alpha_p g^2}{\omega^5}\exp\left(\frac{-20\pi^4}{T_p^4\omega^4}\right)\gamma^{Y_p}, \tag{49}$$

where α_p and Y_p are given as:

$$\alpha_p = \frac{5.061H_s^2}{T_p^4}(1 - 0.287\ln\gamma),$$

$$Y_p = \exp\left(-\frac{1}{2}\left(\frac{\frac{\omega T_p}{2\pi} - 1}{\sigma_p}\right)^2\right),$$

with σ_p as the spectral width parameter given as

$$\sigma_p = \begin{cases} 0.07 \text{ for } \omega \leq \frac{2\pi}{T_p} \\ 0.09 \text{ for } \omega > \frac{2\pi}{T_p}. \end{cases}$$

The relative difference $(\sigma_1^{qs} - \sigma_1)/\sigma_1^{qs}$ of the standard deviation of the maximum dynamic stress along the beam by a quasi-steady and a hydroelastic analysis are plotted in Fig. 10 versus wave peak period T_p for given significant wave heights. The peak periods T_p and significant wave heights are related to the classification of wave exposure as given in NS9415 (2009), see Table 1.

As long as the results are positive, the quasi-static assumption is conservative. From these results alone, the quasi-static assumption appears to be conservative for all stiffnesses and frequencies considered. The degree of conservativity increases with decreasing stiffness EA and increasing peak period T_p. The results do not appear to be particularly sensitive to the wave period.

A very narrow peak response of the stress occurs at the second natural sloshing frequency. It could be expected that the peak in the stress transfer function is visible in the stress standard deviation for irregular waves around $T_p = 5.2$ s which is the second sloshing period. No peaks are visible in the presented results. The narrow peak response contribution to the standard deviation in a sea state can be obtained by evaluating the area of the squared transfer function in the narrow peak response frequency domain and multiplying it with the wave spectrum at the peak frequency. It follows then that the influence on the standard deviation of stress is very small.

To assess if the stress level in itself is reasonable, the most probable largest value, which is roughly four times the standard deviation should be compared to the yield stress. This has not been done. The investigation has only assessed if the method is useable and not if the general stress levels are below the yield stress limit. This is because peak stresses often form around holes and in intersections which has not been modelled here.

5. Conclusions

In this paper the linear theory of a 2D semi-flexible closed fish cage in waves is developed and analysed to investigate the structural response of the semi-flexible closed cage in waves. The results from a 2D case study with relevant full scale dimensions, considering a half circularly shaped semi-flexible closed fish cage with floaters were presented. Investigations only consider the 2D case. However, the findings can be considered a starting point for analysing 3D structures.

We have compared a quasi-static analysis with a fully coupled hydroelastic analysis to investigate if it is a valid and conservative assumption to assume that the stresses in the structure can be assumed quasi-static. We have investigated what happens with the stress in the curved beam part of the closed fish cage for increasing and decreasing stiffness relative to the reference composite structure. One stiffer and two softer cases have been analysed. One major concern for the stresses on a closed cage is the effect of sloshing.

The results indicate that to use the quasi-static assumption is conservative within the given frequency range for all examined stiffnesses and frequencies, except the frequencies very close to the second sloshing frequency. Close to the second sloshing frequency for all the examined stiffnesses, a localised peak can be observed in the coupled hydroelastic results. The second sloshing frequency is a frequency connected to a symmetric sloshing mode. Symmetric sloshing frequencies is not excited by any rigid body motion for an assumed rigid structure, and is therefore not visible in results from a quasi-static analysis. If a symmetrical sloshing eigenperiod is close to the wave peak period, the quasi-steady assumption can be non-conservative dependent on the stiffness of the structure. The analysis should be extended to 3D. It should be investigated if any symmetric sloshing frequencies are in the relevant frequency range for a full-scale cage at hand. Procedures, tables and figures for calculating sloshing frequencies for all these 3D geometries can be found in Faltinsen and Timokha (2009). Fatigue could also be a problem close to symmetric sloshing frequencies, and should be further considered. The response in irregular sea was calculated to find the relevant stress level wave response. These results show no indication of increased stress close to the second sloshing frequency.

Future work should include to generalise the described results to a 3D cage. The results could be extended to 3D using state of the art numerical methods, including the hydroelastic coupling and require dedicated work. Experimental validation is needed. The linear potential flow calculations can be performed by a state-of-the-art method that considers structural deformations. A further step would also be to account for non-linear sloshing, which can lead to swirling and chaos in axisymmetric cages. Since a CFD method is time consuming and viscous effects play a secondary role as long as wave breaking does not occur, the nonlinear multimodal method for potential sloshing flow of an incompressible liquid as described by Faltinsen and Timokha (2009) should be attempted. An additional advantage of the multimodal method is explicit acceleration dependent loads that stabilises numerical time integration in wave–body interaction analysis.

Declaration of competing interest

The authors declare that they have no known competing financial interests or personal relationships that could have appeared to influence the work reported in this paper.

CRediT authorship contribution statement

Ida M. Strand: Conceptualization, Methodology, Software, Writing - original draft, Writing - review & editing. **Odd M. Faltinsen:** Supervision, Writing - review & editing.

Acknowledgments

This work have been financed by the Research Council of Norway through the project "Safe operation of closed aquaculture cages in waves" (grant no. 268402). The work has been carried out at the Centre for Autonomous Marine Operations and Systems (AMOS), supported by the Research Council of Norway through the Centres of Excellence funding scheme, project number 223254 - AMOS. The Norwegian Research Council is acknowledged as the main sponsor of AMOS.

References

Billingham, J., King, A., 2009. Wave Motion. In: Cambridge Texts in Applied Mathematics, Cambridge University Press, Cambridge.
Faltinsen, O.M., 1990. Sea Loads on Ships and Offshore Structures. Cambridge University Press.
Faltinsen, O.M., Timokha, A.N., 2009. Sloshing. Cambridge University Press.
Hanssen, F.-C.W., Bardazzi, A., Lugni, C., Greco, M., 2017. Free-surface tracking in 2D with the harmonic polynomial cell method: Two alternative strategies. Internat. J. Numer. Methods Engrg.
Hanssen, F.W., Greco, M., Shao, Y., 2015. The harmonic polynomial cell method for moving bodies immersed in a Cartesian background grid. In: ASME International Conference on Offshore Mechanics and Arctic Engineering, Vol. 11: Prof. Robert F. Beck Honoring Symposium on Marine Hydrodynamics. http://dx.doi.org/10.1115/OMAE2015-41282.
Ibrahim, R.A., 2005. Liquid Sloshing Dynamics: Theory and Applications. Cambridge University Press, Cambridge.
Kristiansen, D., Lader, P., Endresen, P.C., Aksnes, V., 2018. Numerical and experimental study on the seakeeping behavior of floating closed rigid fish cages. In: ASME 2018 37th International Conference on Ocean, Offshore and Arctic Engineering - Volume 6: Ocean Space Utilization..
Lader, P., Fredriksson, D.W., Volent, Z., DeCew, J., Rosten, T., Strand, I.M., 2015. Drag forces on, and deformation of, closed flexible bags. J. Offshore Mech. Arct. Eng. 137 (August), 041202. http://dx.doi.org/10.1115/1.4030629.
Lader, P., Fredriksson, D.W., Volent, Z., DeCew, J., Rosten, T., Strand, I.M., 2017. Wave response of closed flexible bags. J. Offshore Mech. Arct. Eng. 139 (5), http://dx.doi.org/10.1115/OMAE2016-54146.
Li, S.H., Ren, J.Y., 2018. Analytical study on dynamic responses of a curved beam subjected to three-directional moving loads. Appl. Math. Model. (ISSN: 0307-904X) 58, 365–387. http://dx.doi.org/10.1016/j.apm.2018.02.006, URL http://www.sciencedirect.com/science/article/pii/S0307904X18300763.
Ma, S., Hanssen, F.-C.W., Siddiqui, M.A., Greco, M., Faltinsen, O.M., 2017. Local and global properties of the harmonic polynomial cell method: In-depth analysis in two dimensions. Internat. J. Numer. Methods Engrg. http://dx.doi.org/10.1002/nme.5631.
Malenica, S., Molin, B., Tuitman, J.T., Bigot, F., Senjanovic, I., 2009. Some aspects of hydrostatic restoring for elastic bodies. In: Abstract for 24th IWWWFB, Saint Petersburg, Russia, 2009.
Malenica, S., Vladimir, N., Choi, Y.M., Senjanovic, I., Kwon, S.H., 2015. Global hydroelastic model for liquid cargo ships, In: Seventh International Conference on Hydroelasticity in Marine Technology. Split, Croatia, pp. 493–505.
Newman, J.N., 1994. Wave effects on deformable bodies. Appl. Ocean Res. 16 (1), 47–59. http://dx.doi.org/10.1016/0141-1187(94)90013-2.
NS9415, 2009. Marine Fish Farms - Requirements for Site Survey, Risk Analyses, Design, Dimensioning, Production, Installation and Operation. Norwegian standard, SN / K 509.
Senjanovic, I., Tomic, M., Tomasevic, S., 2008. An explicit formulation for restoring stiffness and its performance in ship hydroelasticity. Ocean Eng. 35 (13), 1322–1338. http://dx.doi.org/10.1016/j.oceaneng.2008.06.004.
Shao, Y., Faltinsen, O.M., 2014a. Fully-nonlinear wave-current- body interaction analysis by a Harmonic Polynomial Cell Method. J. Offshore Mech. Arct. Eng. 136 (August), 8–13. http://dx.doi.org/10.1115/1.4026960.
Shao, Y., Faltinsen, O.M., 2014b. A harmonic polynomial cell (HPC) method for 3D Laplace equation with application in marine hydrodynamics. J. Comput. Phys. 274, 312–332. http://dx.doi.org/10.1016/j.jcp.2014.06.021.
Solaas, F., Rudi, H., Berg, A., Tvinnereim, K., 1993. Floating fish farms with bag pens. In: International Conference on Fish Farming Technology. pp. 317–323.
Strand, I.M., 2018. Sea Loads on Closed Flexible Fish Cages. In: Doctoral Theses at NTNU, vol. 2018:28, Norwegian University of Science and Technology, Faculty of Engineering, Department of Marine Technology, Trondheim.
Strand, I.M., Faltinsen, O.M., 2017. Linear sloshing in a 2D rectangular tank with a flexible sidewall. J. Fluids Struct. 73, 70–81. http://dx.doi.org/10.1016/j.jfluidstructs.2017.06.005.
Strand, I.M., Faltinsen, O.M., 2019. Linear wave response of a 2D closed flexible fish cage. J. Fluids Struct. (ISSN: 0889-9746) 87, 58–83. http://dx.doi.org/10.1016/j.jfluidstructs.2019.03.005.
Strand, I.M., Sørensen, A.J., Volent, Z., 2014. Closed flexible fish cages: modelling and control of deformations. In: Proceedings of 33rd International Conference on Ocean, Offshore and Arctic Engineering. San Francisco, USA, http://dx.doi.org/10.1115/OMAE2014-23059, June 8–13.
Strand, I.M., Sørensen, A.J., Volent, Z., Lader, P., 2016. Experimental study of current forces and deformations on a half ellipsoidal closed flexible fish cage. J. Fluids Struct. 65, http://dx.doi.org/10.1016/j.jfluidstructs.2016.05.011.
Tan, Y., Shao, Y., Read, R., 2019. Coupled motion and sloshing analysis of a rigid cylindrical closed fish cage in regular waves, In: Proceedings of the 38th International Conference on Ocean, Offshore and Arctic Engineering - OMAE. Vol. 6, Glasgow, Scotland, UK.
Ventsel, E., 2001. Thin Plates and Shells : Theory, Analysis, and Applications. Marcel Decker, New York.
Yang, Y., Kuo, S., 1987. Effect of curvature on stability of curved beams. J. Struct. Eng. 113 (6), 1185–1202. http://dx.doi.org/10.1061/(ASCE)0733-9445(1987)113:6(1185).